Asteroid moons a.k.a. satellites

List of moons...

- Johnston (2021), Margot etal. (2015), Marchis etal. (2008a,b)
- http://www.johnstonsarchive.net/astro/asteroidmoons.html

- **467 in total** (!)
- 85 NEAs
- 31 Mars-crossers
- 209 MBAs
- 6 Jupiter Trojans
- 116 TNOs

Discovery

Johnston (2021)

lightcurves (MB)

adaptive optics (MB)

Hubble (TNOs)

imaging

occultations

radar (NEAs)

astrometry

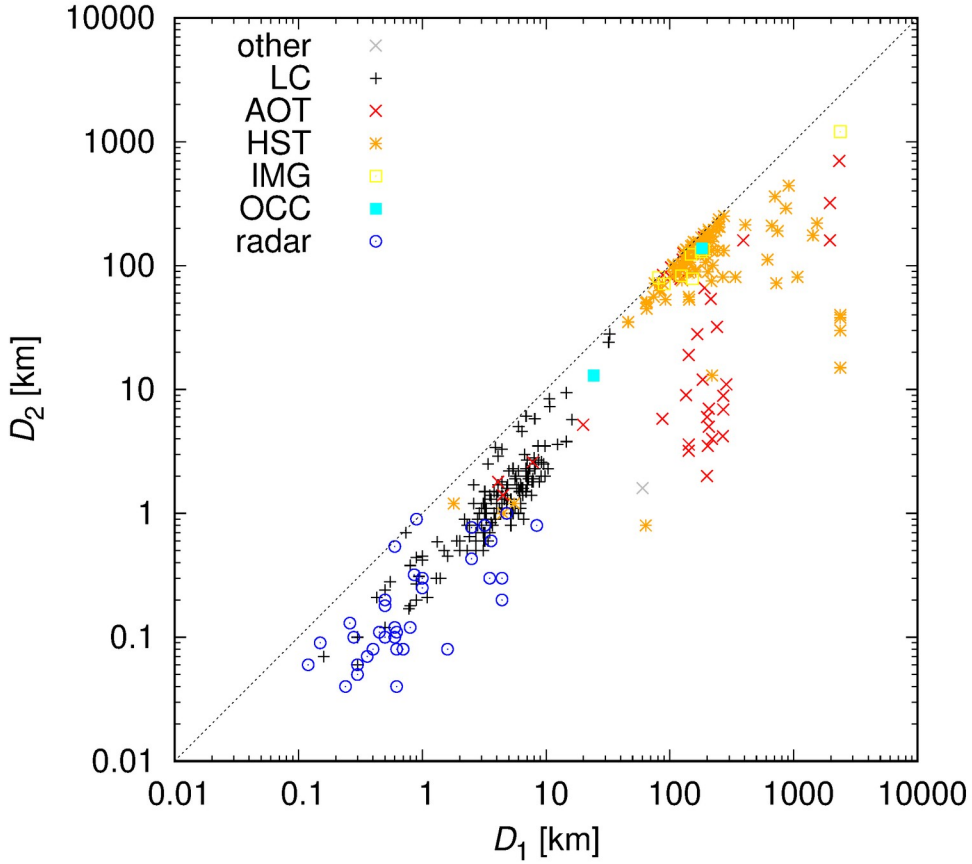

Pravec etal. (2012)

lightcurve w. eclipses

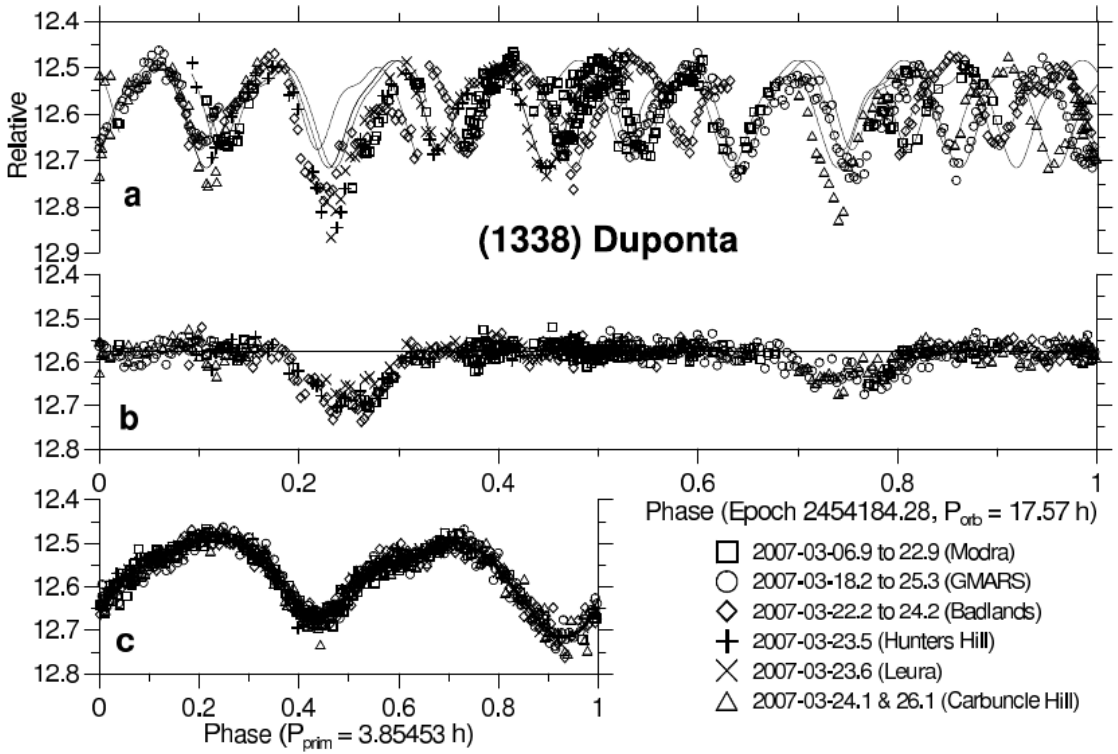

Fig. 2.— Lightcurve data of (1338) Duponta, which has a secondary-to-primary diameter ratio of about 0.24. (a) The original data showing both lightcurve components, folded with the orbit period. (b) The orbital lightcurve component, derived after subtraction of the primary lightcurve component, showing the mutual events between components of the binary system. (c) The primary lightcurve component. Figure from Pravec et al. (2012).

Margot etal. (2015)
Doppler ↔ delay ↕
spike due to secondary
w. synchronous rotation

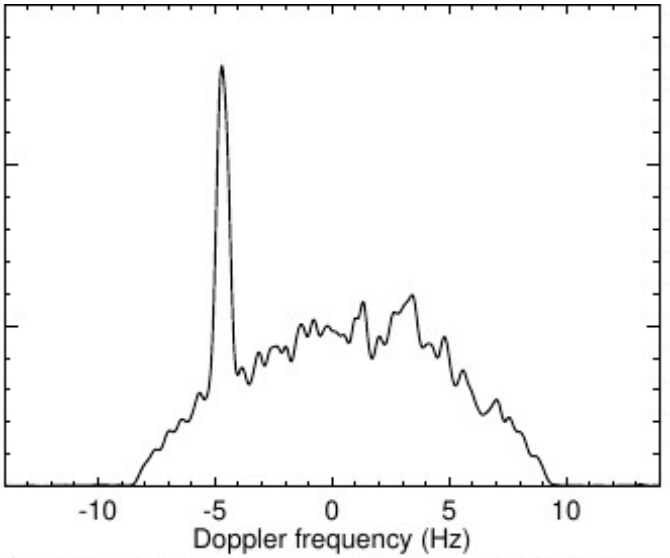

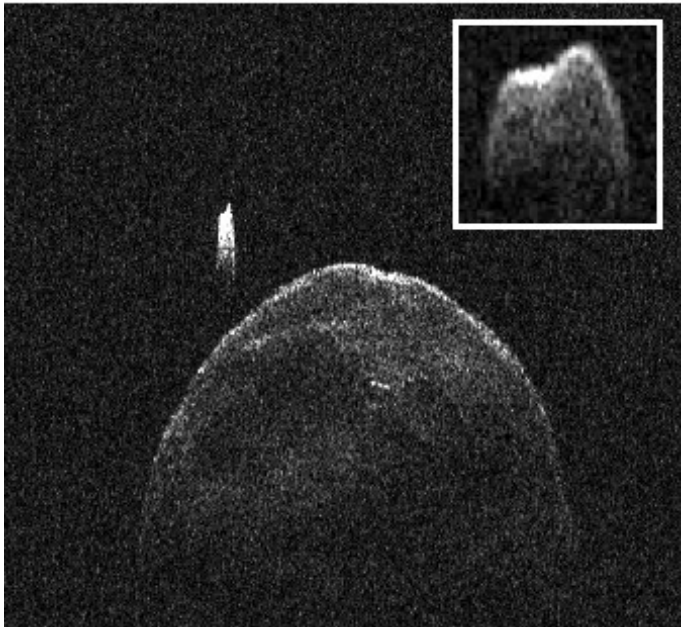

Marchis etal. (2021)
adaptive optics
halo subtraction

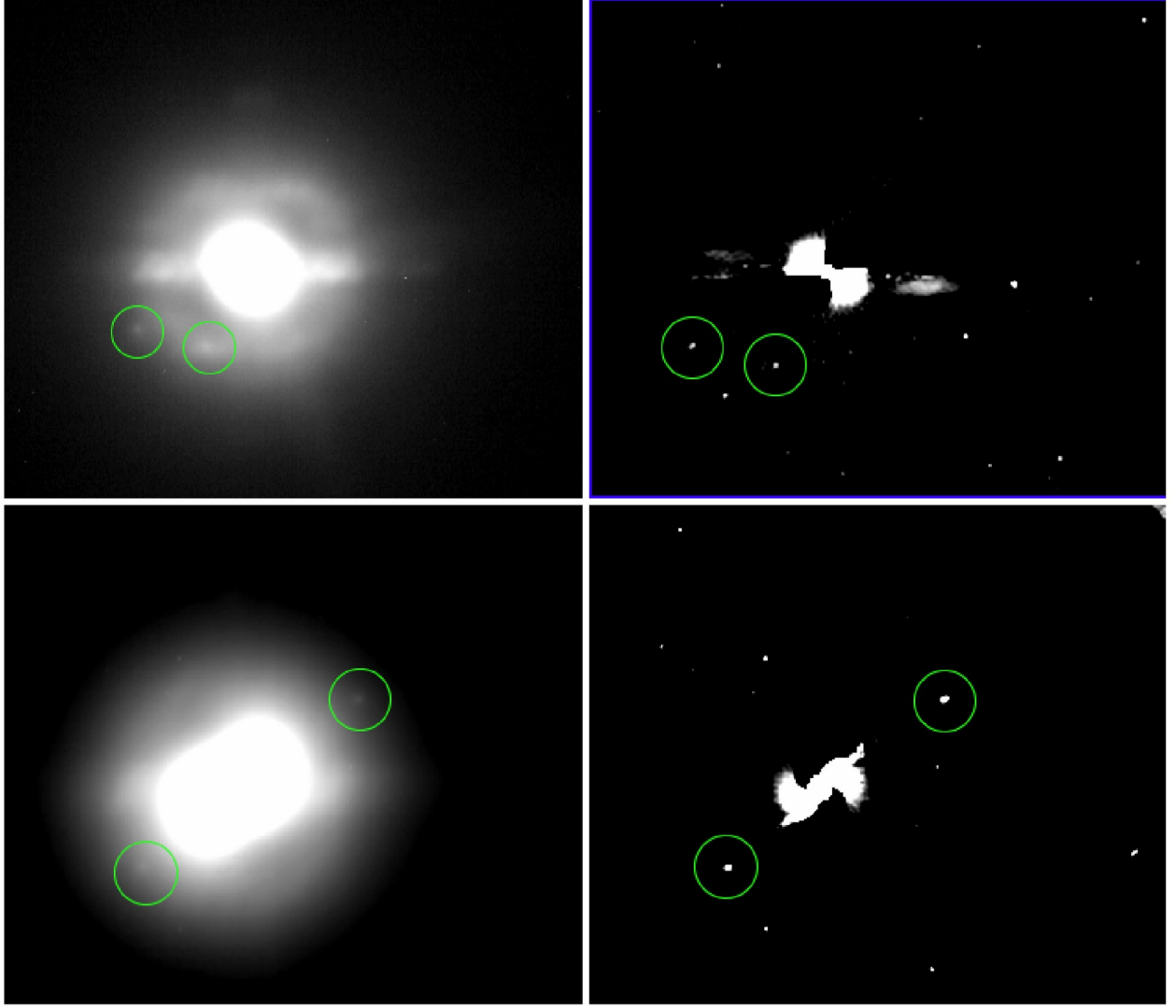

Fig. 3. Processed ZIMPOL images on the *left*, revealing the presence of the satellites, CleoSelene and AlexHelios around (216) Kleopatra at two epochs (*bottom*: 2017-07-14, *top*: 2017-08-22). To reveal the moons which are as faint as the halo (due to imperfect AO correction), we subtracted a rotational average of the image centered on the primary (*right image*). The circle points to the location of the satellites in the images. The other dots in the images are bad pixels.

Primary vs. secondary size

- typical ratios:
- MB 0.3
- TNOs upto 1.0
- small moons

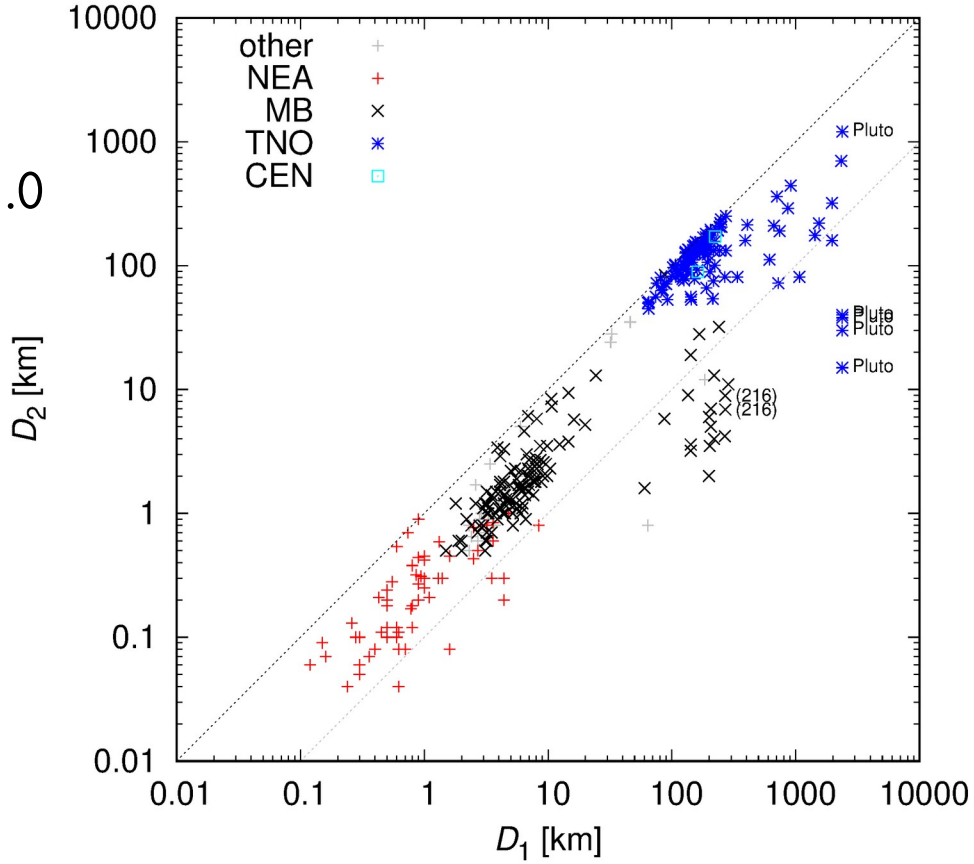

Primary vs. secondary mass

- dtto, 3 orders

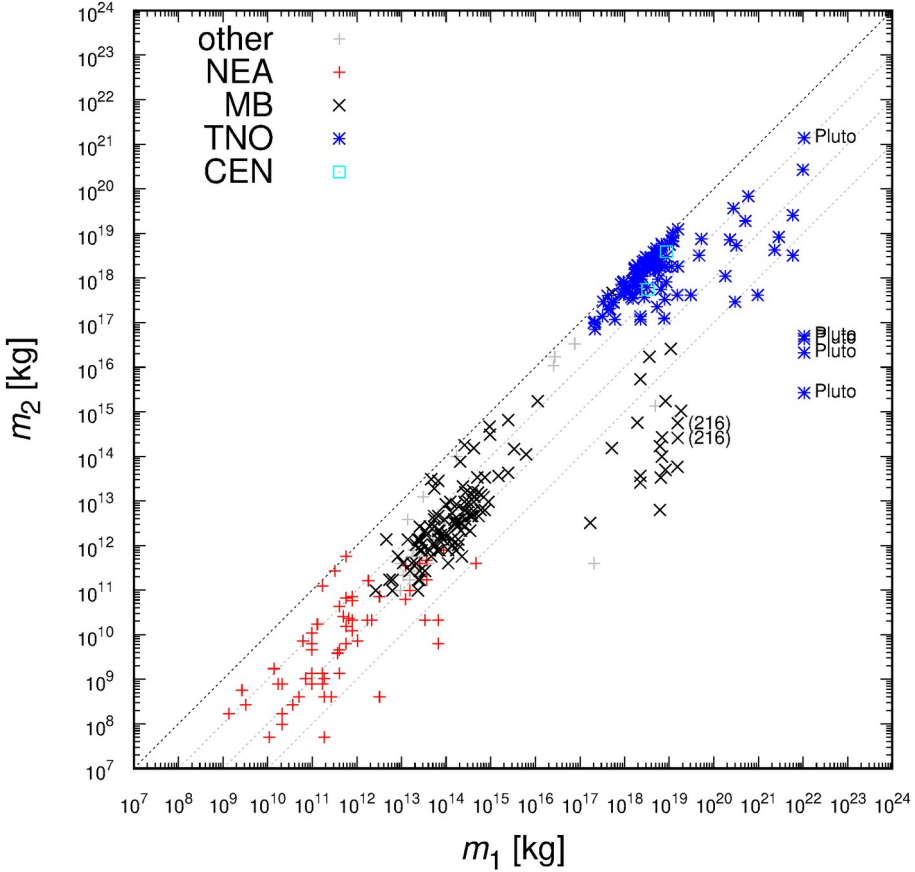

Primary size vs. size ratio

Johnston (2021)
Lindsay etal. (2014)
A ... small asteroid
B ... small binary
C ... contact binary
L ... large asteroid
W ... wide binary

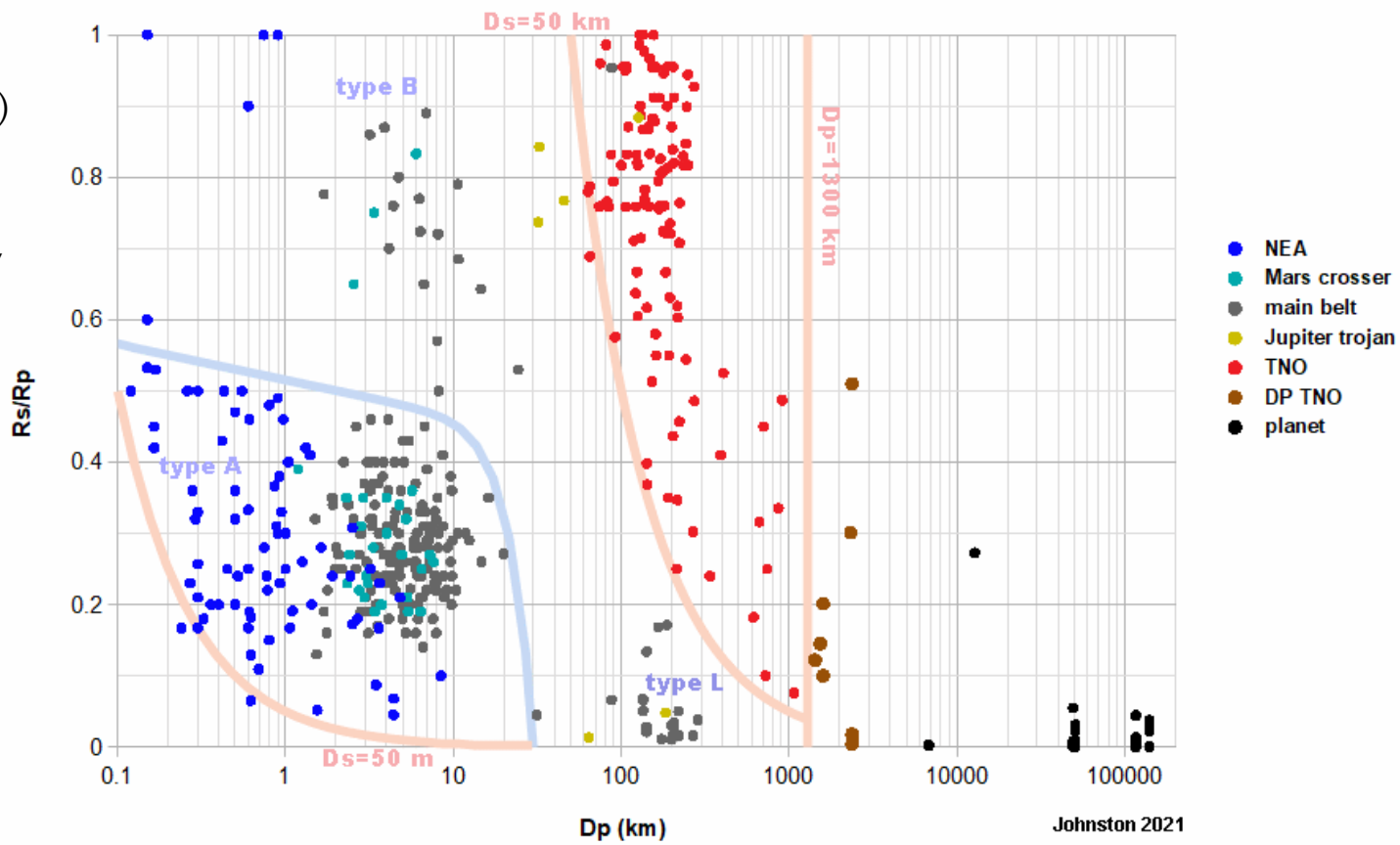

Period vs. eccentricity

- unconstrained e, strong bias?
- populations:
- eccentric TNOs, cf. origin?
- few MB w. e > 0.01
- few Trojans
- low e < 0.01, or zero?
- very useful for *geodesy*!

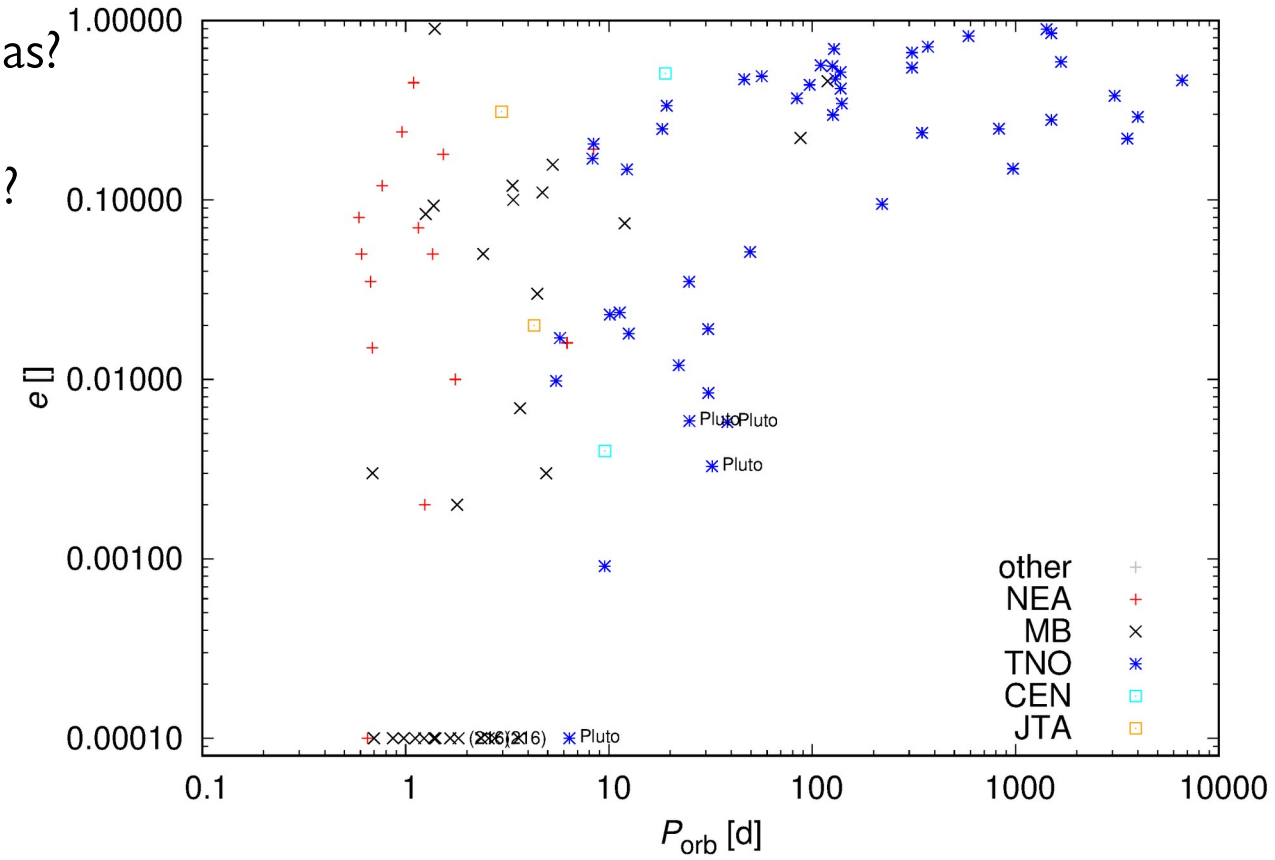

Primary size vs. spin rate

- LCDB (Warner & Harris)
- NEAs mostly *sub-critical*
- **MB** dtto
- big TNOs more spread
- few slow-rotators
- no fast-rotators
- *not* random sampling?

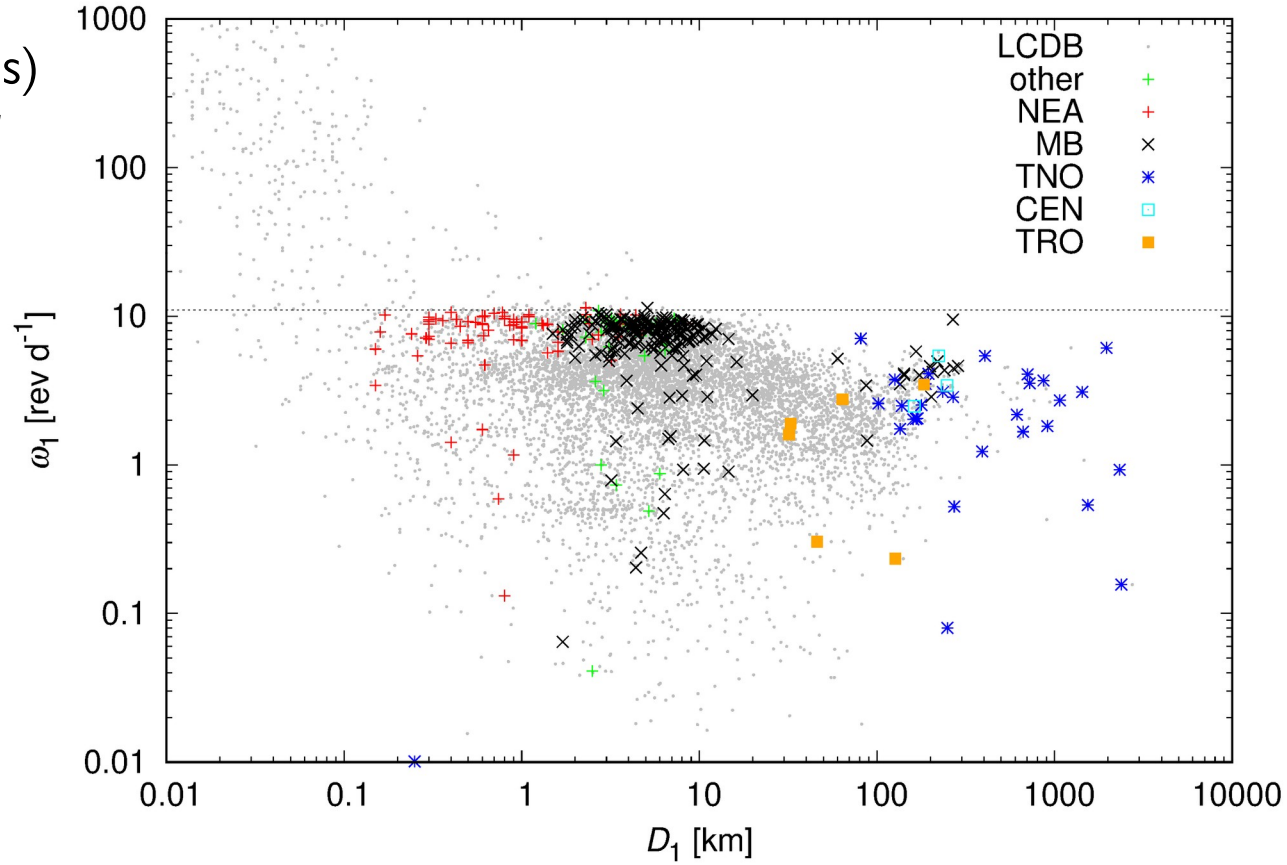

Examples: (22) Kalliope

- **Linus**, massive moon™, D = 166 km, d = 28 km (cf. Antiope, Patroclus)
- P = (3.595606 ± 0.000375) d, long arc, **158** positions (AO 2001-2019)
- Vachier etal. (2012), Drummond etal. (2021), Marin etal. (in prep.)

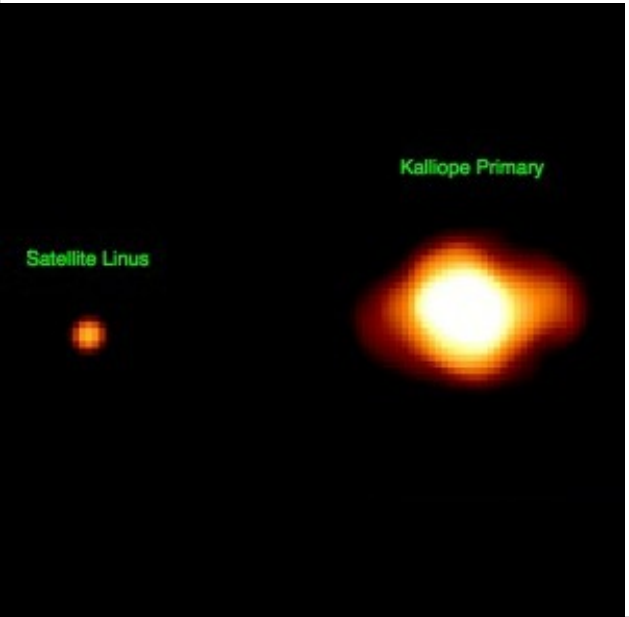

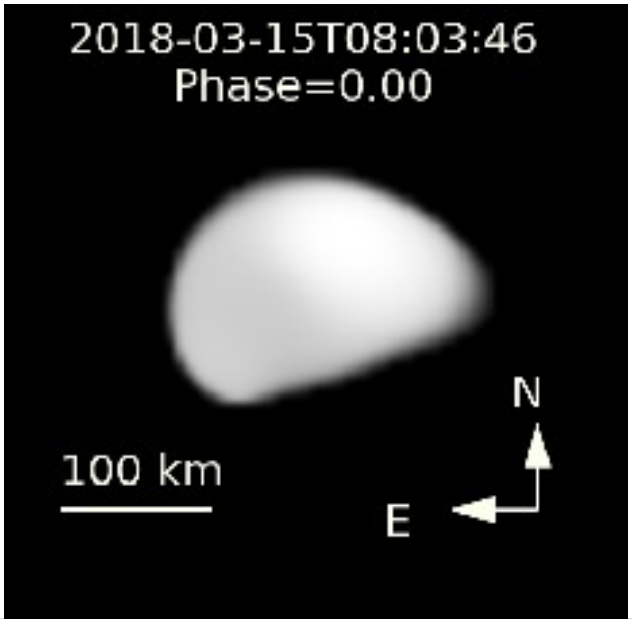

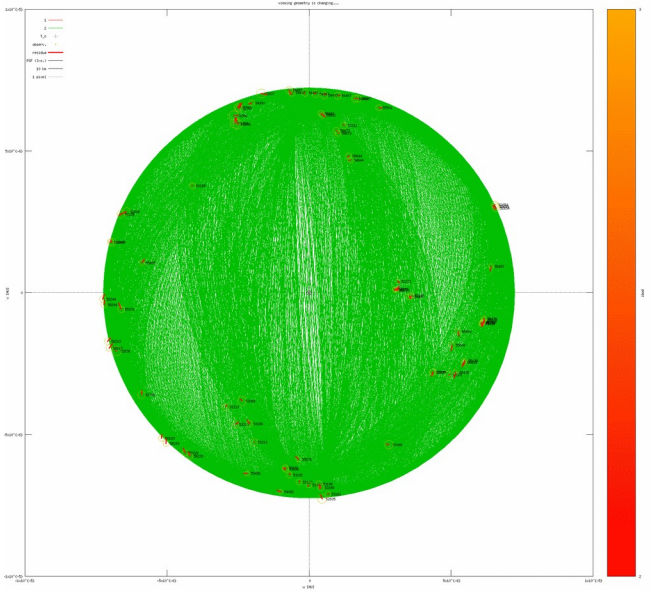

(45) Eugenia

- Petit-Prince, S/2004 (45) 1
- eccentric orbits, $e_1 = 0.0020 \pm 0.0012$, $e_2 = 0.11 \pm 0.02$, geodesy (!)
- Marchis etal. (2010), model w. mutual interactions

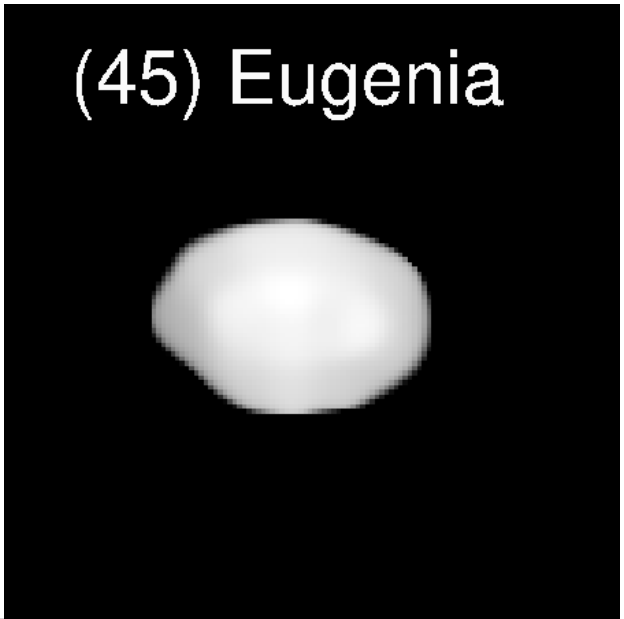

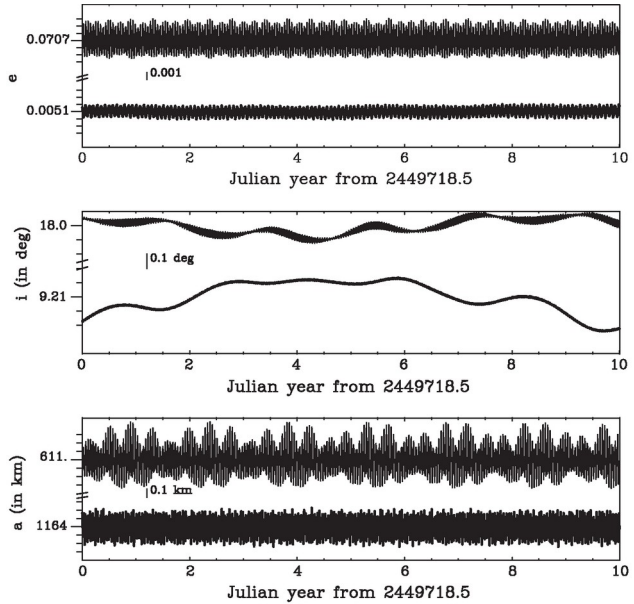

(87) Sylvia

- Romulus, and Remus
- P = 1.35699 and 3.64126 d, inclined orbits, i_1 = 8.7 deg, i_2 = 7.4 deg, geodesy (!)
- Carry etal. (2021); some problems w. differentiation (!)

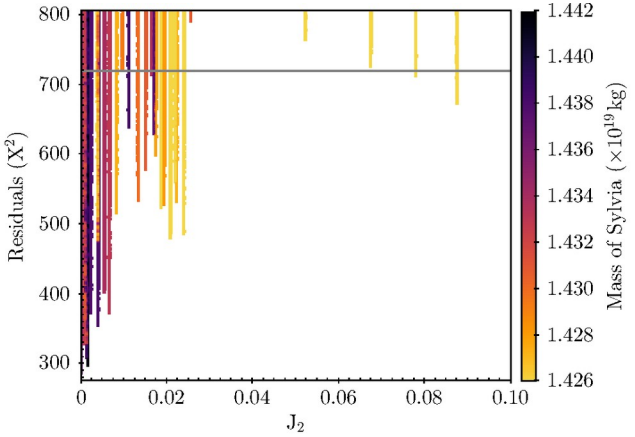

Fig. 4: Orbital residuals (χ^2) as function of the dynamical quadrupole J_2. The horizontal grey line corresponds to the χ^2 providing a fit at 1 σ of the observations.

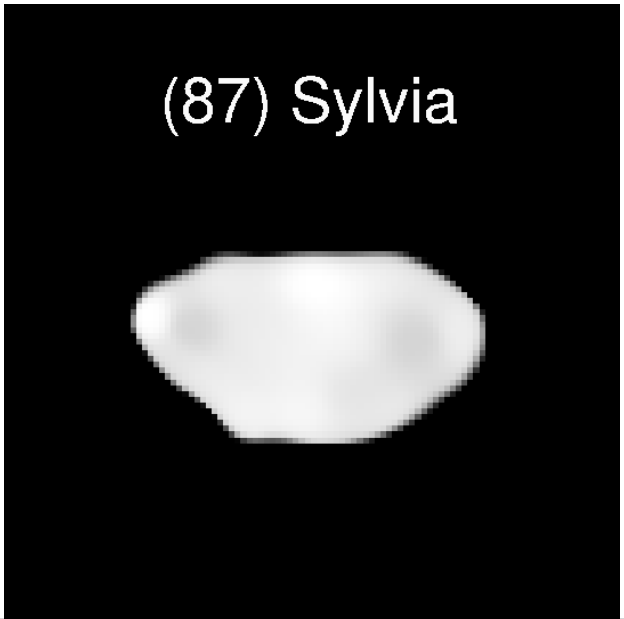

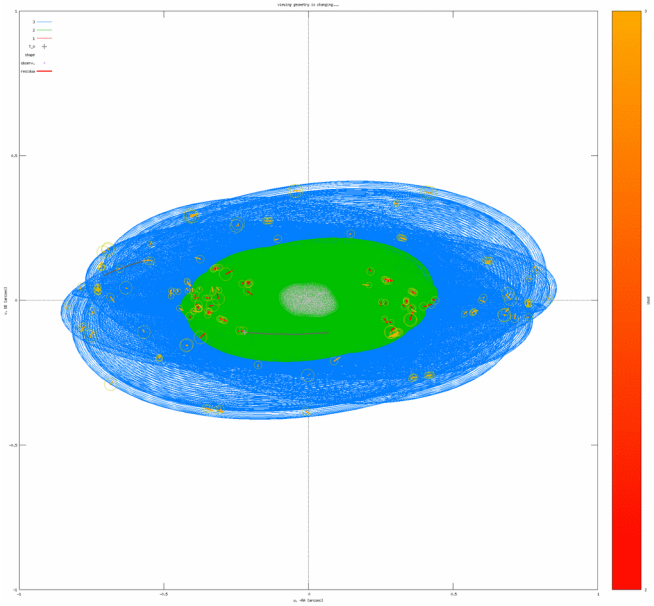

(130) Elektra

- S/2014 (130) 1, S/2003 (130) 1
- P = 1.256 and 5.287 d, eccentric orbits, $e_1 = 0.157 \pm 0.036$, $e_2 = 0.0835 \pm 0.0096$
- Marchis etal. (2008b), Yang etal. (2016), Vernazza etal. (2021)

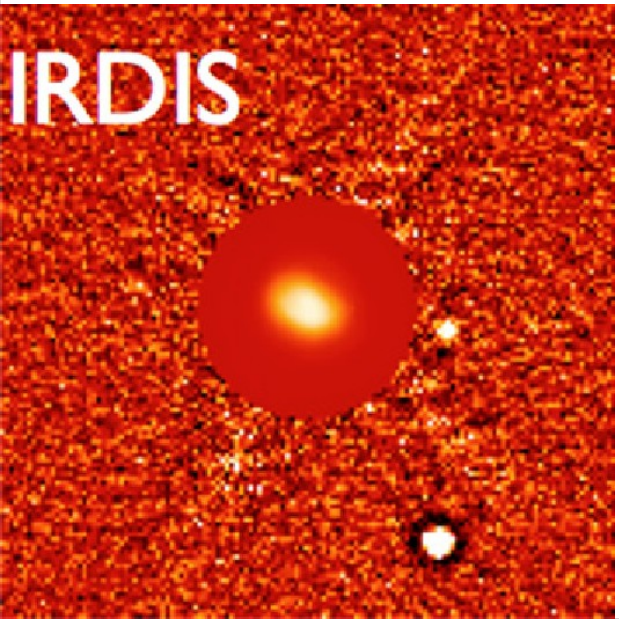

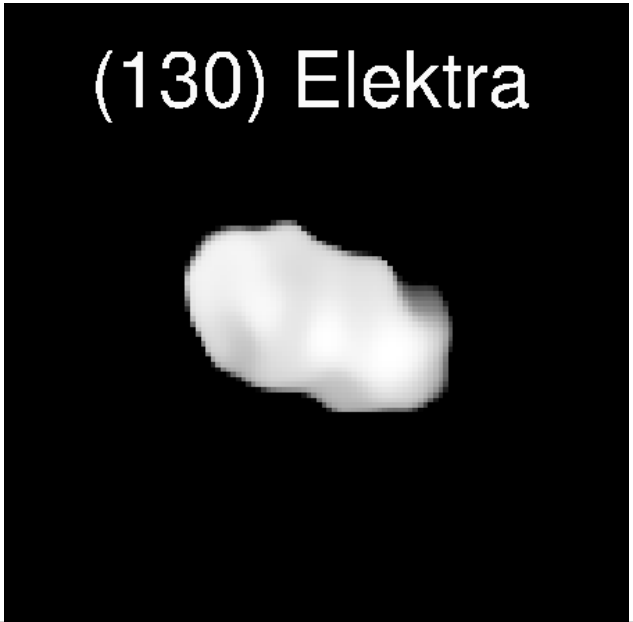

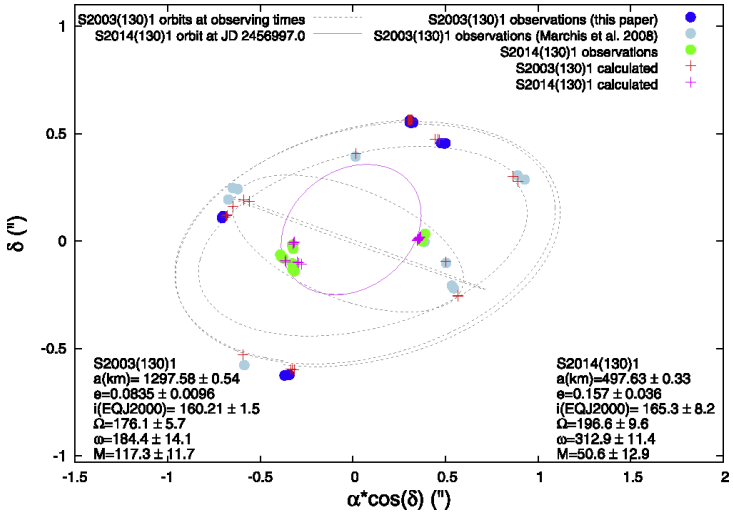

(216) Kleopatra

- Cleoselene, Alexhelios
- significant revision of P_1, P_2, M, V, ϱ & re-interpretation (!)
- Descamps etal. (2011), Marchis etal. (2021), Brož etal. (2021ab), ESO PR...

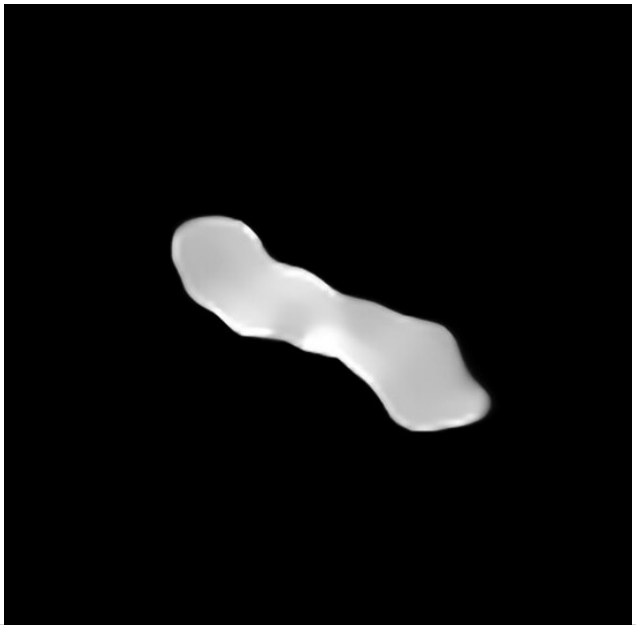

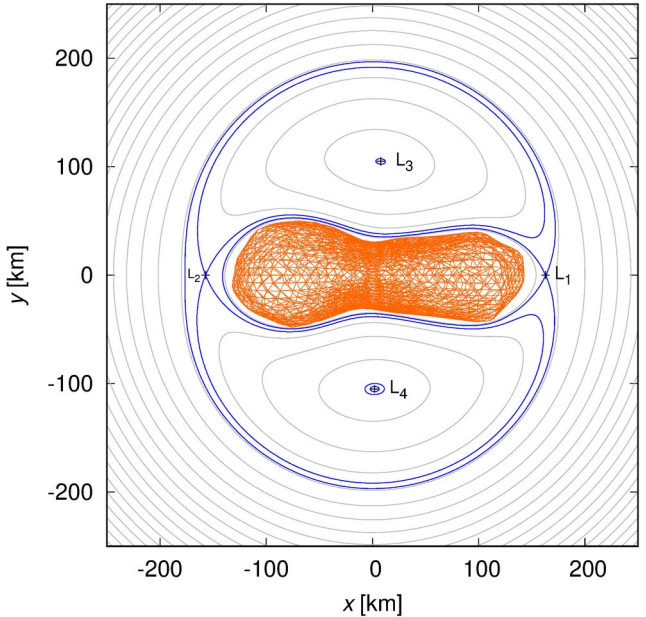

(90) Antiope

- equal-size binary (Merline etal. 2000), cf. (617) Patroclus
- sequence: sphere → Maclaurin (2-axial) → Jacobi (3-axial) → dumbbell → binary

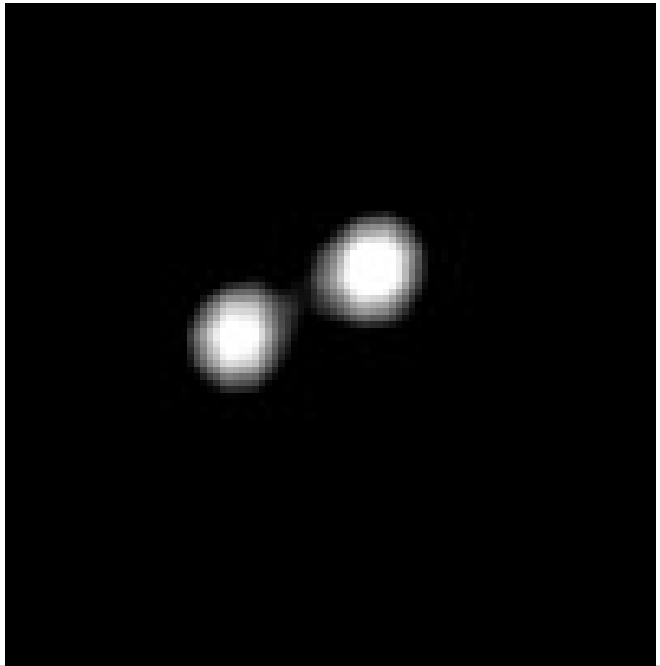

Other interesting cases...

- (617) Patroclus - Jovian Trojan (see Lucy)
- (5261) Eureka - Martian Trojan, family
- (10188) Chariklo - Centaur w. ring system (Braga-Ribas etal. 2014)
- (136108) Haumea - TNO w. 1 ring + 2 moons (Ortiz etal. 2017)
- (486958) Arrokoth - contact binary, “lenticular” (McKinnon etal. 2020)
- ...

Origins

- L: catastrophic disruptions (SMATs; Durda etal. 2004)
- L: escaping-ejecta binaries (EEBs)
- cratering events?
- S: YORP effect spin-up (Cuk & Burns 2005)
- S: collisional spin-up
- ejections from *critical* rotators? (e.g. Kleopatra; Brož etal. 2021a)
- reaccretion from ring? (cf. Chariklo, Haumea)
- streaming instability, aerodynamic drag (McKinnon etal. 2020)
- tidal disruption (cf. SL9)

Dynamics

- post-fission encounters (high *e*; Fang etal. 2011)
- Kozai cycles ($e \leftrightarrow i$; Perets & Naoz 2009)
- close encounters w. planets (Fang & Margot 2012)
- spin-orbit interactions of irregulars (Scheeres etal. 2006)
- chaotic rotation (Naidu & Margot 2015)
- tidal evolution of rubble-piles (Goldreich & Sari 2009)
- tidal saltation ("dunes"; Harris etal. 2009)
- **BYOPR** radiative effect (Cuk & Burns 2005)
- tidal/radiative equilibrium (Jacobson & Scheeres 2011)
- reflex motion (radar; Margot etal 2002)
- ...

Pairs

Vokrouhlický & Nesvorný (2008)
metrics $d = na[(\Delta a/a)^2 + ...]^{1/2}$ [m s^{-1}]
statistical argument!

Pravec etal. (2010), Scheeres (2007)
fast primary rotation
strength-less bodies
$\omega_{crit} = (4/3\ \pi G \varrho)^{1/2}$
$\omega_q = \omega_{crit}\ [(1 + q)/(1 + q^{1/3})^3]^{1/2}$

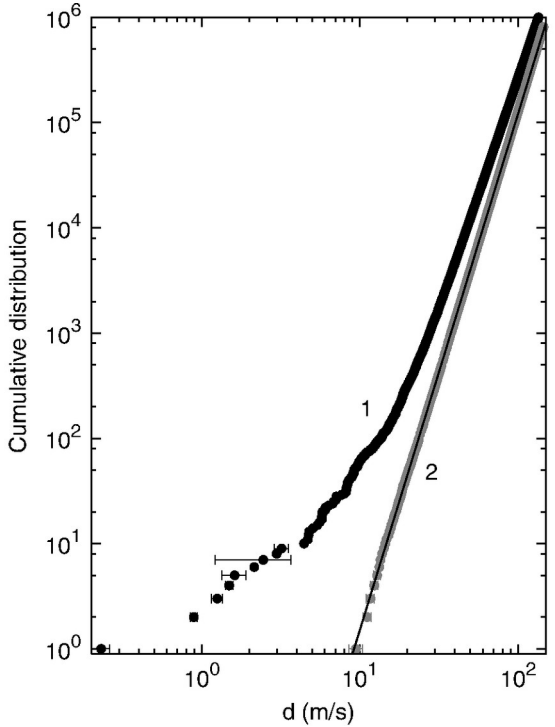

Figure 1. The cumulative number of pairs as a function of d; $N(<d)$. The black symbols labeled 1 denote the distribution of real asteroids. The error bars associated with d values of the ten tightest pairs were estimated by their orbit uncertainties. The gray symbols labeled 2 show the distribution obtained by selecting 370,000 test orbits with $1.7 < a < 3.6$ AU. The associated error bars denote uncertainties determined from several such test distributions (see Section 4). The best-fit power law to blue symbols is $N(<d) \propto d^{4.91}$ (straight line).

Pairs

Jacobson & Sheeres (2011)

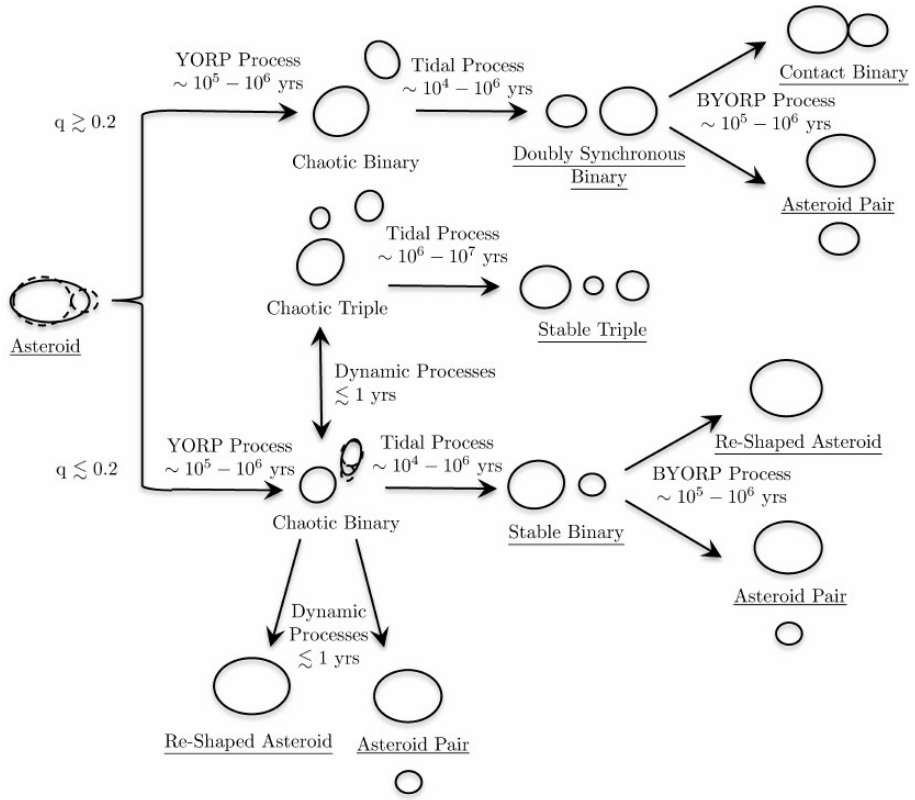

Fig. 11.— Flowchart showing the possible evolutionary paths for an asteroid after it undergoes rotational fission. Each arrow is labeled with the dominant process and an estimated timescale for this process. Underlined states are nominally stable for a YORP effect timescale. Figure from Jacobson and Scheeres (2011b).

Vokrouhlický etal. (2021)

(18777) Hobson family
incl. pair ... + (57738)
collisional disruption
w. suitable geometry
→ low-velocity dispersal
→ unbound pair

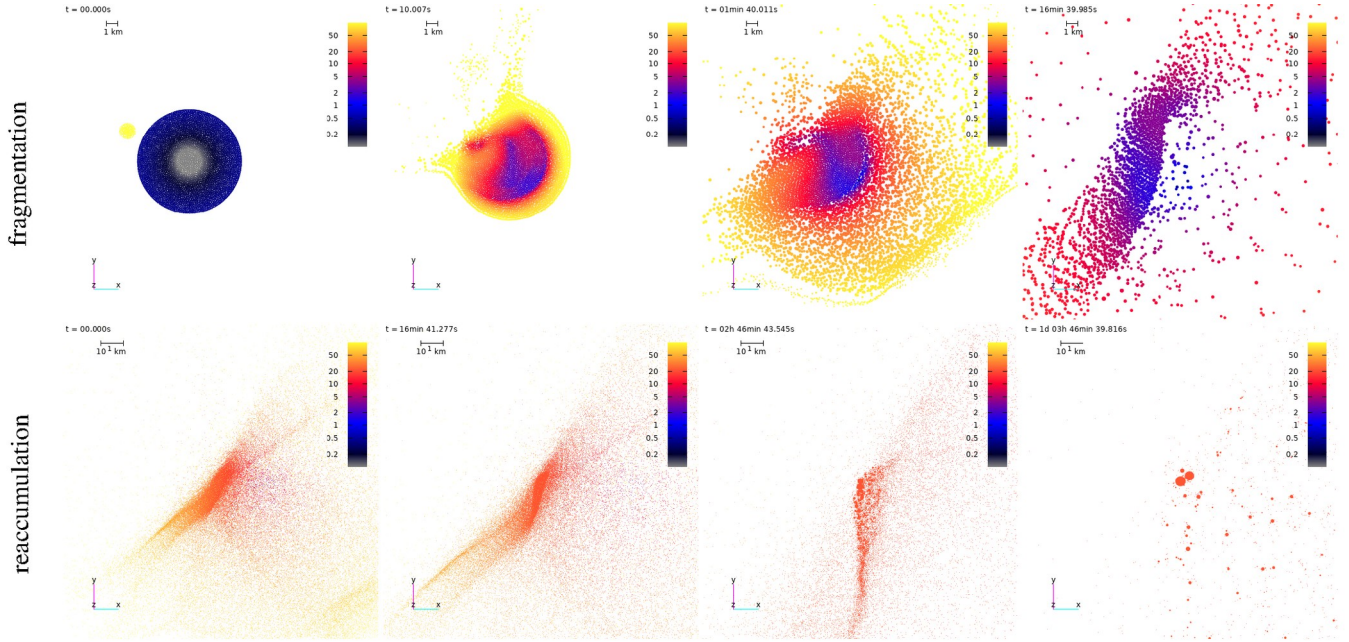

Fig. 8. Snapshots from an SPH/*N*-body simulation of a single parent body breakup. The basic parameters were a target size $D_{\rm tar} = 9$ km, an impactor size $D_{\rm imp} = 1.3$ km, an impact angle $\phi = 30°$ ("near-to-head-on situation"), and an impact velocity $v = 5$ km s^{-1}. The fragmentation phase is shown for the epochs $t = 0, 10, 100, 10^3$ s (*top*, *a–d from left to right*), and the reaccumulation phase for $t = 0, 10^3, 10^4, 10^5$ s (after handoff; *bottom*, *e–h from left to right*). The spatial distribution of SPH particles is plotted only within a limited range of the coordinate $z \in (-1, 1)$ km to clearly show the interior structure of the parent body, its damage, and the clump formation zones. Colors correspond to the velocity v in m s^{-1} relative to the target body (scale shown using the bar). Individual panels can be described as follows: (*a*) the initial conditions, (*b*) high-speed ejecta formed at the impact site, (*c*) formation of a cavity with low relative speeds, (*d*) deformation of the target, (*e*) handoff phase, (*f*) streams of high speed, individual particles escaping from the system, (*g*) ongoing reaccumulation, and (*h*) formation of an unbound, nearly equal-size pair accompanied by the subkilometer fragments. (Animation is available online and at https://sirrah.troja.mff.cuni.cz/~mira/hobson/hobson.html).

Durda etal. (2004)

- SMATs
- EEBs

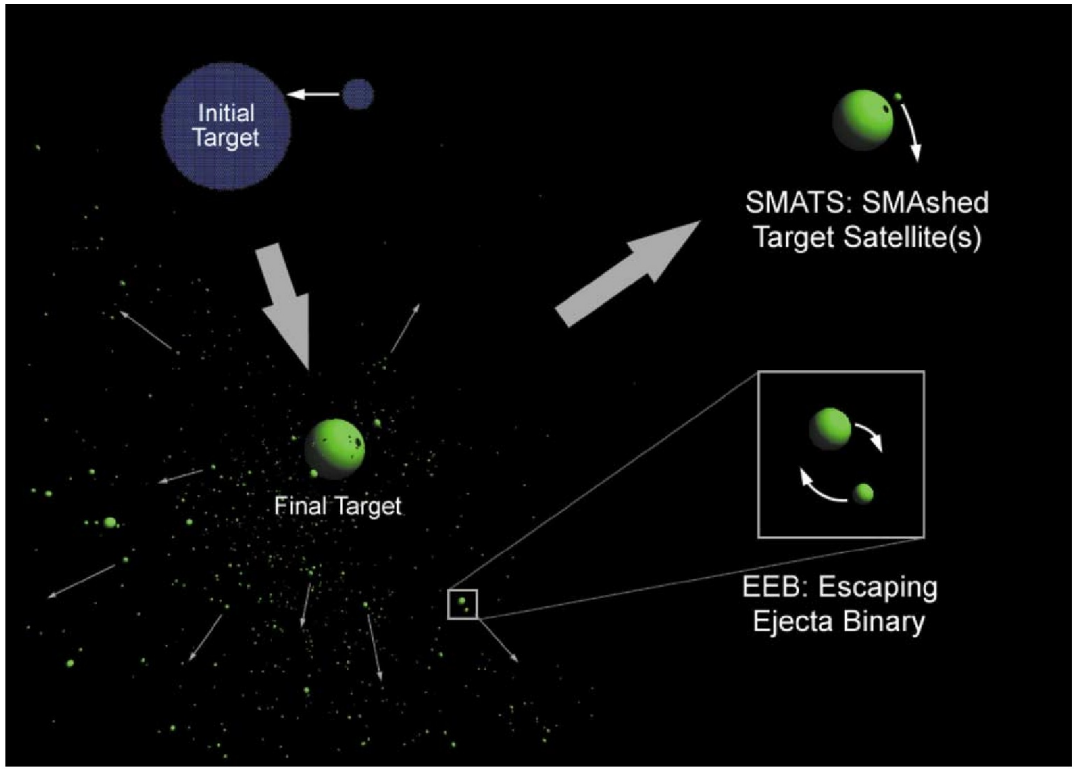

Fig. 1. Two classes of satellites resulting from large impacts between asteroids. SMAshed Target Satellites (SMATS) form from impact debris that enters into orbit around the remaining target body, which is a gravitationally reaccreted rubble pile. Escaping Ejecta Binaries (EEBs) result when smaller fragments escaping the impact site have similar trajectories, such that they become gravitationally bound to one another.

Nesvorný etal. (2019)

- streaming instability (SI), rotating clumps, aerodynamic drag → spiralling
- prograde/retrograde ratio = 0.8, in accord w. observations

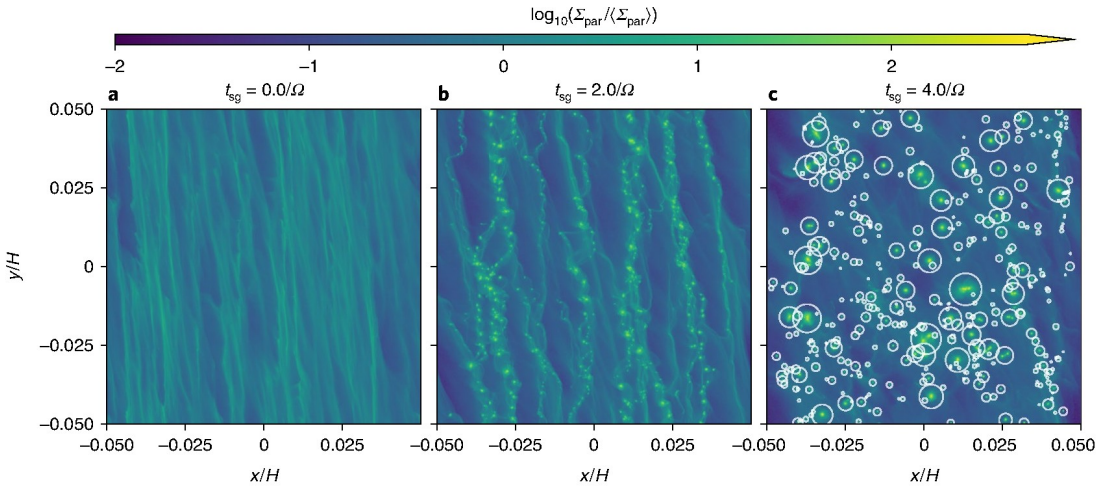

Fig. 1 | Three snapshots from our 3D simulation of the SI where the nonlinear particle clumping triggers gravitational collapse into planetesimals. The plots show the vertically integrated density of solids (Σ_{par}), projected on the disk plane, relative to the initially uniform surface density ($\langle\Sigma_{par}\rangle$). The x and y coordinates show the shearing-box dimensions in units of the gas disk scale height, H (the Sun is to the left; the orbital velocity vector points up). Time t increases from left to right as labelled ($t_{sg} = t - t_0$; particle self-gravity was switched on at $t_0 = 36/\Omega$). **a**, Azimuthal filaments have already formed at $t_{sg} = 0$. **b**,**c**, The filaments fragment into gravitationally bound clumps. The circles in **c** depict the Hill spheres of clumps that were identified by the PLAN algorithm. The full evolution is shown in the Supplementary Video.

Scheirich etal. (2021)

- LC (eclipses) measurements of quadratic mean anomaly:
- (66391) 1999 KW4: (–0.65 ± 0.16) deg/yr^2, a ↑ i.e. BYORP + tides?
- (88710) 2001 SL9: (2.8 ± 0.2) deg/yr^2, a ↓ "pure" BYORP
- (175706) 1996 FG3: compatible w. *zero*, in equilibrium?

Vernazza etal. (2021)

- AO survey of large asteroids (MB), both S- and C-types, C- featureless, “fluid”

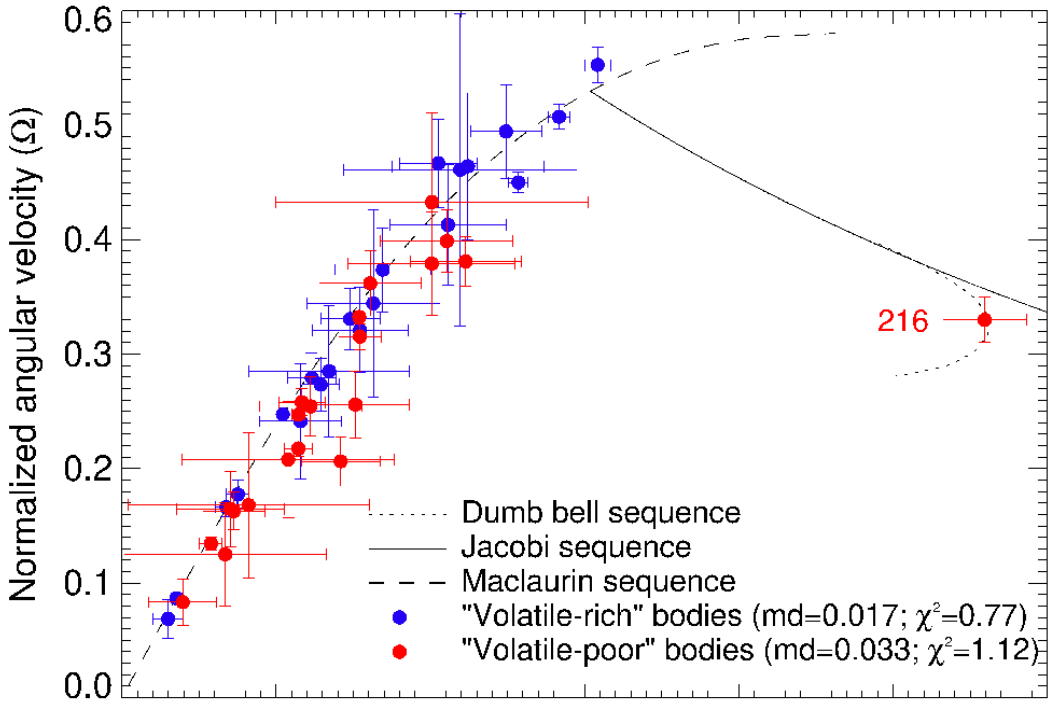

Vernazza etal. (2021)

- shapes from AO + LC + radar (Viikinkoski etal. 2015, Jorda etal. 2016), volumes
- masses from moons, or mutual encounters (Fienga etal. 2020)

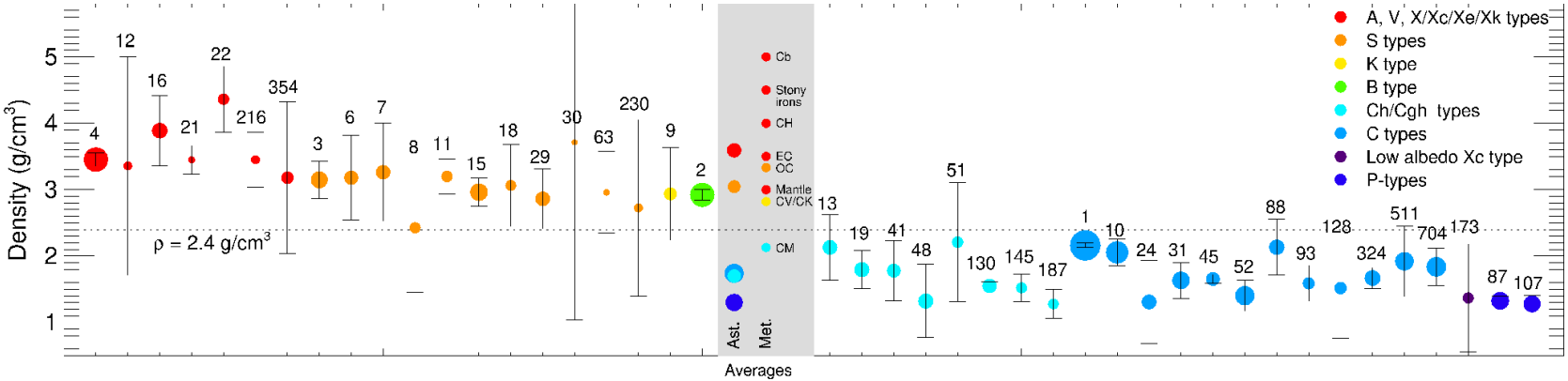

Fig. 7. Density distribution of our large programme asteroid targets. The density distribution appears strongly bimodal (see text) with volatile-poor bodies on the left of the gray zone and volatile-rich bodies on its right. Two multiple systems (93 Minerva and 107 Camilla; Marchis et al. 2013; Pajuelo et al. 2018) imaged outside of our observing program were also added because of their accurate density determination. Asteroids are grouped following their spectral classification. The relative sizes of the dots follow the relative diameters of the bodies in logarithmic scale. Error bars are one sigma. In the center of the figure, the gray zone shows the average density of the main asteroid groups (left) and of their likely meteoritic analogs (right).

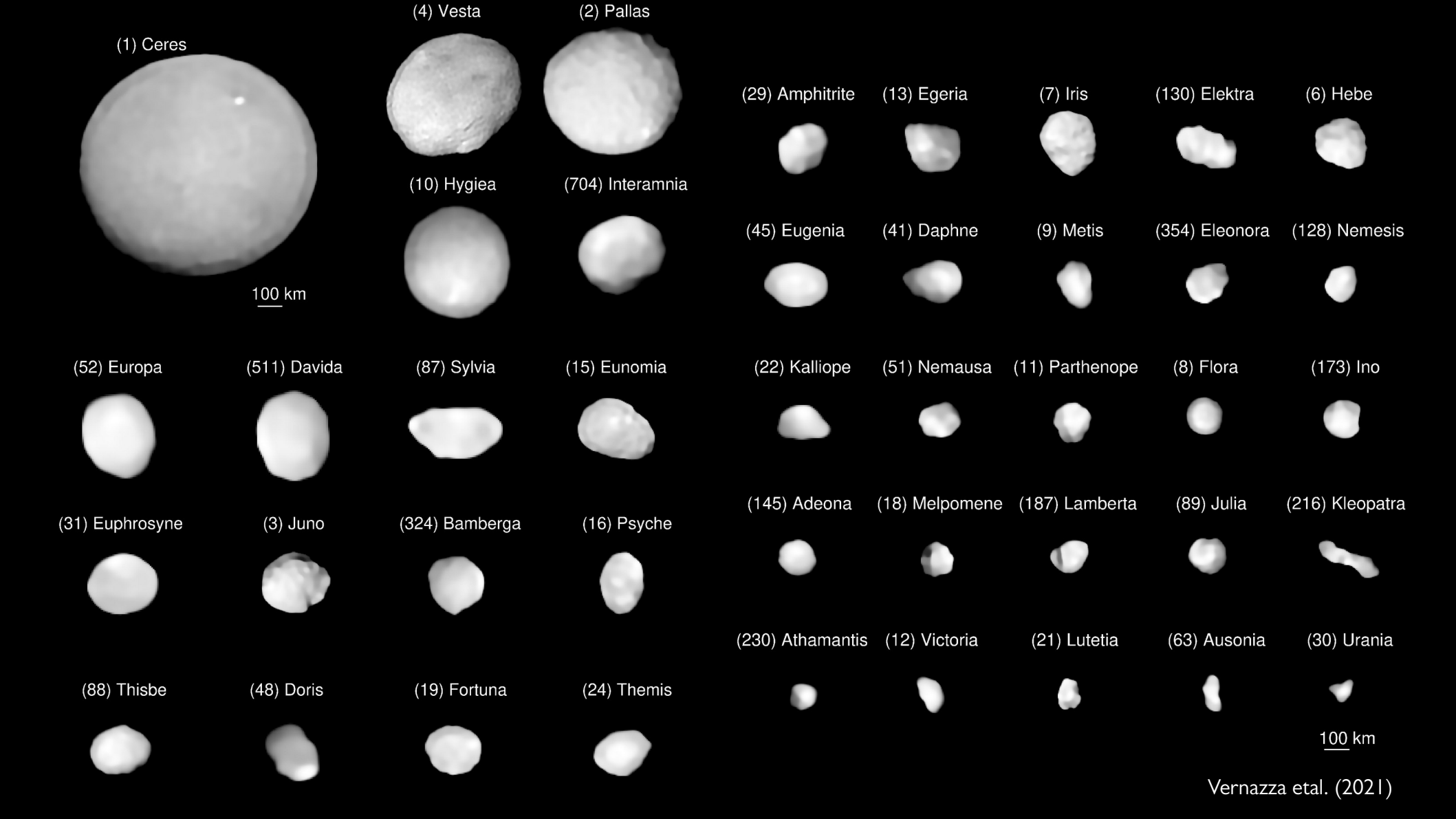
(1) Ceres
(4) Vesta
(2) Pallas
100 km
(10) Hygiea
(704) Interamnia
(29) Amphitrite
(13) Egeria
(7) Iris
(130) Elektra
(6) Hebe
(45) Eugenia
(41) Daphne
(9) Metis
(354) Eleonora
(128) Nemesis
(52) Europa
(511) Davida
(87) Sylvia
(15) Eunomia
(22) Kalliope
(51) Nemausa
(11) Parthenope
(8) Flora
(173) Ino
(31) Euphrosyne
(3) Juno
(324) Bamberga
(16) Psyche
(145) Adeona
(18) Melpomene
(187) Lamberta
(89) Julia
(216) Kleopatra
(88) Thisbe
(48) Doris
(19) Fortuna
(24) Themis
(230) Athamantis
(12) Victoria
(21) Lutetia
(63) Ausonia
(30) Urania
100 km
Vernazza etal. (2021)

Links

- https://sirrah.troja.mff.cuni.cz/~mira/tmp/kleopatra/kleopatra.html
- https://sirrah.troja.mff.cuni.cz/~mira/tmp/kleopatra/moons.html
- https://sirrah.troja.mff.cuni.cz/~mira/tmp/kleopatra/sphere2018.html
- https://sirrah.troja.mff.cuni.cz/~mira/tmp/kleopatra/resonance32.html
- https://sirrah.troja.mff.cuni.cz/~mira/tmp/sylvia/sylvia.html
- https://sirrah.troja.mff.cuni.cz/~mira/tmp/sylvia/silhouettes.html
- https://sirrah.troja.mff.cuni.cz/~mira/tmp/sylvia/shape.html
- https://sirrah.troja.mff.cuni.cz/~mira/tmp/kalliope/kalliope.html